frontiers | Frontiers in Earth Science

TYPE Original Research
PUBLISHED 19 June 2023
DOI 10.3389/feart.2023.1217304

OPEN ACCESS

EDITED BY
Mingtao Li,
Linyi University, China

REVIEWED BY
Xing Jian,
Xiamen University, China
Zezhang Song,
China University of Petroleum, China

*CORRESPONDENCE
Ping Guan,
pguanl@pku.edu.cn

RECEIVED 05 May 2023
ACCEPTED 31 May 2023
PUBLISHED 19 June 2023

CITATION
Li S, Liu P, Guan P, Zhang D, Xia X, Ding X, Zhang C, Zhang J and Tang J (2023), Eocene to Miocene paleoclimate reconstruction of the northern Tibetan Plateau: constraints from mineralogy, carbon and oxygen isotopes of lacustrine carbonates in the western Qaidam Basin. *Front. Earth Sci.* 11:1217304. doi: 10.3389/feart.2023.1217304

Eocene to Miocene paleoclimate reconstruction of the northern Tibetan Plateau: constraints from mineralogy, carbon and oxygen isotopes of lacustrine carbonates in the western Qaidam Basin

Shien Li[1], Peixian Liu[1], Ping Guan[1]*, Daowei Zhang[2], Xiaomin Xia[2], Xiaonan Ding[1], Chi Zhang[1], Jihua Zhang[1] and Jianzhou Tang[3]

[1]Ministry of Education Key Laboratory of Orogenic Belts and Crustal Evolution, School of Earth and Space Sciences, Peking University, Beijing, China, [2]Research Institute of Exploration and Development, Qinghai Oilfield Company, PetroChina, Dunhuang, China, [3]College of Geology and Environment, Xi'an University of Science and Technology, Xi'an, China

The Cenozoic climatic evolution of the Tibetan Plateau (TP), together with its driving mechanism, have been a subject of interest for decades. This study presents detailed sedimentology, mineralogical (XRD), carbon, and oxygen isotope analyses of lacustrine deposits from the Eocene to the Miocene in the western Qaidam Basin, the northern TP. The petrological observation and XRD data of 109 samples reveal that the sediments are composed of mixed siliciclastic, carbonate, and evaporate minerals. And the carbonate isotopic results show negative $\delta^{13}C$ (–7.49‰ to –3.41‰) and negative to slightly positive δ^{18} values (–14.65‰ to 0.2‰). Both isotopes display a positive correlation with the contents of carbonates and evaporates, which suggests that evaporation is the major controlling factor of carbon and oxygen isotope. Therefore, the isotopes can be used as reliable indicators of the intensity of evaporation for paleoclimatic reconstruction. The reconstruction results reveal three distinct arid stages: top of the lower Xiaganchaigou Formation to the upper Xiaganchaigou Formation (ca.40-32 Ma), bottom of the Xiayoushashan Formation (ca.22-20 Ma), top of the Shangyoushashan Formation (ca.13-8.2 Ma). We suggest that the aridity during ~40-32 Ma may have been related to the regression of the Paratethys Sea and uplift of the TP, while the aridity during 22-20 Ma may have been caused by the uplift and denudation of the mountains around the basin. The aridity after ~13 Ma could be attributed to both global cooling and tectonic events in the northern TP. Furthermore, by comparing the climate records of the Qaidam Basin with those of other basins in Central Asia, a regional correlation can be established between different basins during the first and third drought stages. This study reveals that during the Eocene to Miocene, the climate change between different regions in the Qaidam Basin was synchronized and had a good connection with the surrounding basins, which responded to global climate change and regional tectonic activities.

KEYWORDS

northern margin of Tibetan Plateau, Qaidam Basin, cenozoic, carbon and oxygen isotopes, climate evolution

1 Introduction

Due to the complex global climate change and regional tectonism, the evolutionary history and driving mechanisms of the Cenozoic climate in Asia have been a provocative topic for decades (Ramstein et al., 1997; Wang et al., 1999; Guo et al., 2008; Xiao et al., 2010; Li et al., 2018; Wu et al., 2022). Global climate has experienced drastic changes from early extreme greenhouse environments during the early Cenozoic to the current ice chamber climate, with the north and south poles covered by ice and snow (Zachos et al., 2001; Westerhold et al., 2020). Global climate has a profound impact on vapor transport efficiency and global sea-level change (Li et al., 2018; Bao et al., 2019; Page et al., 2019). The Cenozoic collision in the Eurasian continent formed the TP and changed the distribution of land-sea (Harrison et al., 1992; Pan, 1999; Yin and Harrison, 2000; Tapponnier et al., 2001; Wang et al., 2008). The strong rain shadow effect caused by the uplift of the plateau severely shaped the climatic processes in Central Asia (Dettman et al., 2003; Kent-Corson et al., 2009; Hough et al., 2011; Zhuang et al., 2011; Wang et al., 2020). In addition, the shrinking and westward migration of the ocean that once reached as far as the southern margin of the Tarim Basin (TB) profoundly changed the climate and environmental evolution of Central Asia (Ramstein et al., 1997; Bosboom et al., 2014a; Bougeois et al., 2018; Kaya et al., 2019; Wang et al., 2019). The TP experienced multiple periods of climate change during the Cenozoic. Factors such as global climate cooling, the uplift of the TP, and the regression of the Paratethys are considered the major driving factors of climate change in this region. However, the underlying mechanism for climate change is poorly understood and contentious, and it is difficult to compare the influence of each driving factor in different stages of the Cenozoic (Dupont-Nivet et al., 2007; Jian et al., 2013; Song et al., 2020). Evidence in this regard needs to be supplemented and improved.

The Qaidam Basin is a key region for understanding the history and the mechanism for climate change because the basin hosts successive sedimentary strata ranging from the Paleocene to the Quaternary in which valuable climatic and environmental information has been preserved; the lacustrine carbonates and evaporite deposits within these strata are highly sensitive to climate variation and thus can be effective paleoclimate archives. Geologists have done extensive work in sedimentology (Dupont-Nivet et al., 2007; Li et al., 2018; Bougeois et al., 2018), stable isotopes (Graham et al., 2005; Kent-Corson et al., 2009; Rieser et al., 2009; Zhuang et al., 2011; Yuan et al., 2015; Li et al., 2016; Li et al., 2017; Ma et al., 2017; Song et al., 2017; Liu et al., 2021; Xiong et al., 2021), and paleontology (Wang et al., 1999; Dupont-Nivet, 2008; Miao et al., 2011; Miao et al., 2013; Song et al., 2020) in this area. The paleoclimate reconstruction can enhance our knowledge of the Asian aridification and the uplift of the Tibetan Plateau. However, due to the uneven distribution of strata, most previous studies have focused only on outcrops from the edge of the basin which limited research to a specific stage without long-term quantification. And the previous studies mostly focused on the interior of the basin and lacked comparison with the surrounding areas.

In continental environments both isotopes, particularly oxygen, are thought to be associated with evaporation (Talbot, 1990; Li and Ku, 1997; Leng and Marshall, 2004); thus, they are recognized to determine the type of paleolake basin (Talbot, 1990; Li and Ku, 1997; Benavente et al., 2019), paleosalinity (Yuan et al., 2015), paleolake-level evolution (Ricketts and Anderson, 1998; Saez and Cabrera, 2002; Bristow et al., 2012)and paleoclimate evolution (Leng and Marshall, 2004; Caves et al., 2014; Wang et al., 2020). This study reconstructs the history of climate change in the Qaidam Basin from the Eocene to Miocene based on detailed petrographic observations and mineralogical and stable isotopic data of lacustrine carbonates in the western Qaidam Basin. The studied interval (43.8–8 Ma) covers a long period during the Cenozoic, thus providing a rare opportunity to evaluate the impact of different controlling factors on the northern TP.

2 Geologic setting and age constraints

The Qaidam Basin is located in the northern margin of the TP, with an average elevation of 3 km, and is bounded by the Altyn Mountains to the northwest, the Qilian Mountains to the northeast, and the East Kunlun Mountains to the south (Figure 1A). Cenozoic strata within the Qaidam Basin have been subdivided into eight stratigraphic units: the Lulehe Fm. (E_{1+2}), the lower Xiaganchaigou Fm. (E_3^1), the upper Xiaganchaigou Fm. (E_3^2), the Shangganchaigou Fm. (N_1), the Xiayoushashan Fm. (N_2^1), the Shangyoushashan Fm. (N_2^2), the Shizigou Fm. (N_2^3), and the Qigequan Fm. (Q) (Guan and Jian, 2013). This study focuses primarily on the western part of the basin. It was constrained by the India–Eurasia collision and the subsequent multi-stage uplift of the TP. During the early Eocene (Lulehe Fm.), orogeny occurred due to the long-distance effect of the collision, and a coarse-grained alluvial fan system was widely developed in the basin (Fu et al., 2012). From the lower Xiaganchaigou Fm. (the end of the Eocene) to the Shangyoushashan Fm. (the Miocene, when the TP uplifted remarkably), a fine-grained sedimentary system developed in the western Qaidam Basin with a less active structural background (Li et al., 2017; Cheng et al., 2021).

Due to the lack of widely developed tuff in the continental sediments in the northern TP, the absolute age of the strata has not been obtained. As the field research gradually deepened, magnetostratigraphy has been widely applied in different areas of the basin, greatly improving the understanding of the age of Cenozoic sedimentary rocks in the Qaidam Basin (Sun et al., 2005; Fang et al., 2007; Lu and Xiong, 2009; Ji et al., 2017; Wang et al., 2017; Nie et al., 2019). Given the limitations of discontinuous drilling cores, the chronological framework based on field magnetostratigraphy is employed herein. There are two contrasting debated age models of Cenozoic strata in the Qaidam Basin. The traditional model assigns a Paleocene basal age to the Cenozoic strata in the basin, despite minor uncertainties in the absolute age of the boundaries between adjacent stratigraphic units (Sun et al., 2005; Zhang, 2006; Fang et al., 2007; Lu and Xiong, 2009; Wang et al., 2012; Ji et al., 2017; Li et al., 2020a). The new age model claims for an Oligocene initial deposition (Wang et al., 2017; Nie et al., 2019). In view of the above huge differences, some studies compared the above two models through the deformation history and climatic reconstruction, suggesting that the traditional age model maybe more reasonable (Sun et al., 2020; Cheng et al., 2021). Therefore, we choose the traditional age model of the Hongliugou

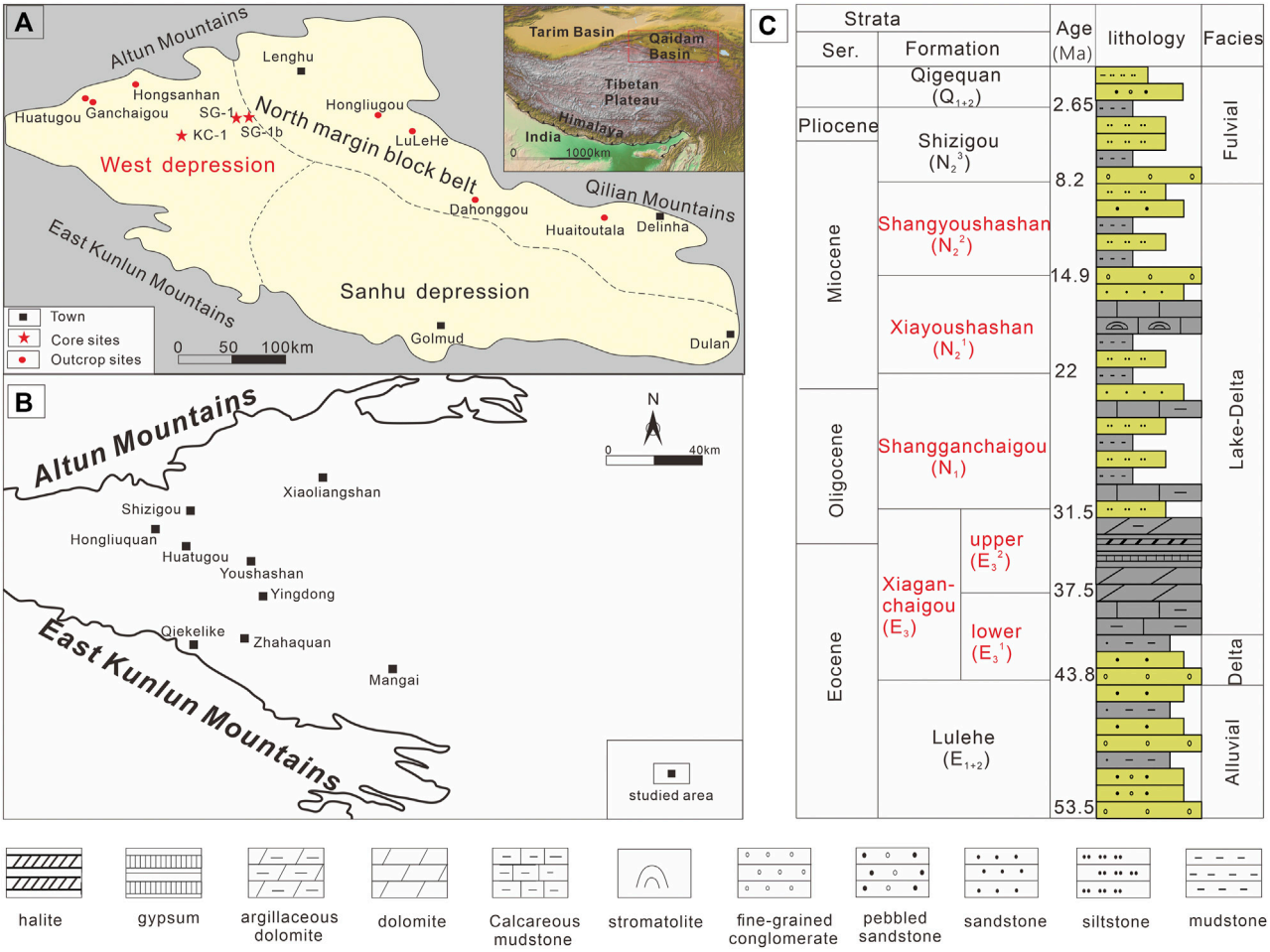

FIGURE 1
(A) Tectonic units of the Qaidam Basin and location of previous studies within the basin [modified from Zhang et al. (2018)]; **(B)** Samples distribution area of this study; **(C)** Schematic stratigraphic column of the western Qaidam Basin.

section, whose geochronological data provides a good correlation with the adjacent Xining Basin (Dai et al., 2006; Fang et al., 2019; Li et al., 2020a). The stratigraphic units and corresponding age intervals involved in this study (Figure 1C) are as follows: the Lower Xiaganchaigou Fm. (43.8–37.5 Ma), the upper Xiaganchaigou Fm. (37.5–31.5 Ma), the Shangganchaigou Fm. (31.5–22 Ma), the Xiayoushashan Fm. (22–14.9 Ma), and the Shangyoushashan Fm. (14.9–8.2 Ma). The stratigraphic division and sedimentary sequence in the studied area primarily come from seismic stratigraphic and logging-data-based stratigraphic correlations of the Qinghai Oilfield.

3 Methods and materials

This study included 109 samples from the Eocene to Miocene in the western Qaidam Basin. The samples were gathered from drilling cores in eight contiguous areas (Figure 1B) covering the Cenozoic strata from the E_3^1 to the N_2^2. It was difficult to obtain continuous samples covering all Cenozoic strata in the same area or well due to the uneven distribution of strata in the basin. Thus, samples from different areas adjacent to each other in the basin were spliced according to the sequence of strata to conduct systematic research in chronological order. The main steps of sample splicing were: 1) the proportion of the sample in the corresponding formation was determined according to the depth of each sample and the top and bottom depth of the formation; each sample was assigned a specific age according to the top and bottom age constraints of the formation (specific formation ages in the previous section); 2) bases on specific ages, the sequence of samples was determined; samples were arranged from old to new to ensure the sedimentary sequence between and within formations (It was assumed that the deposition rate of each formation was relatively constant, which is acceptable when correlating different formations over a long time range). Detailed age data of the samples are shown in Supplementary Table S1. The distribution areas of the 109 core samples are indicated as follows (Figure 1B): E_3^1 samples are primarily from Qiekelike, only one from Hongliuquan; E_3^2 samples are from Shizigou in Yingxi; N_1 samples are from Zhahaquan; N_2^1 samples are primarily from Youshashan and Yingdong; N_2^2 samples are primarily from Xiaoliangshan, Youshashan, and Yingdong.

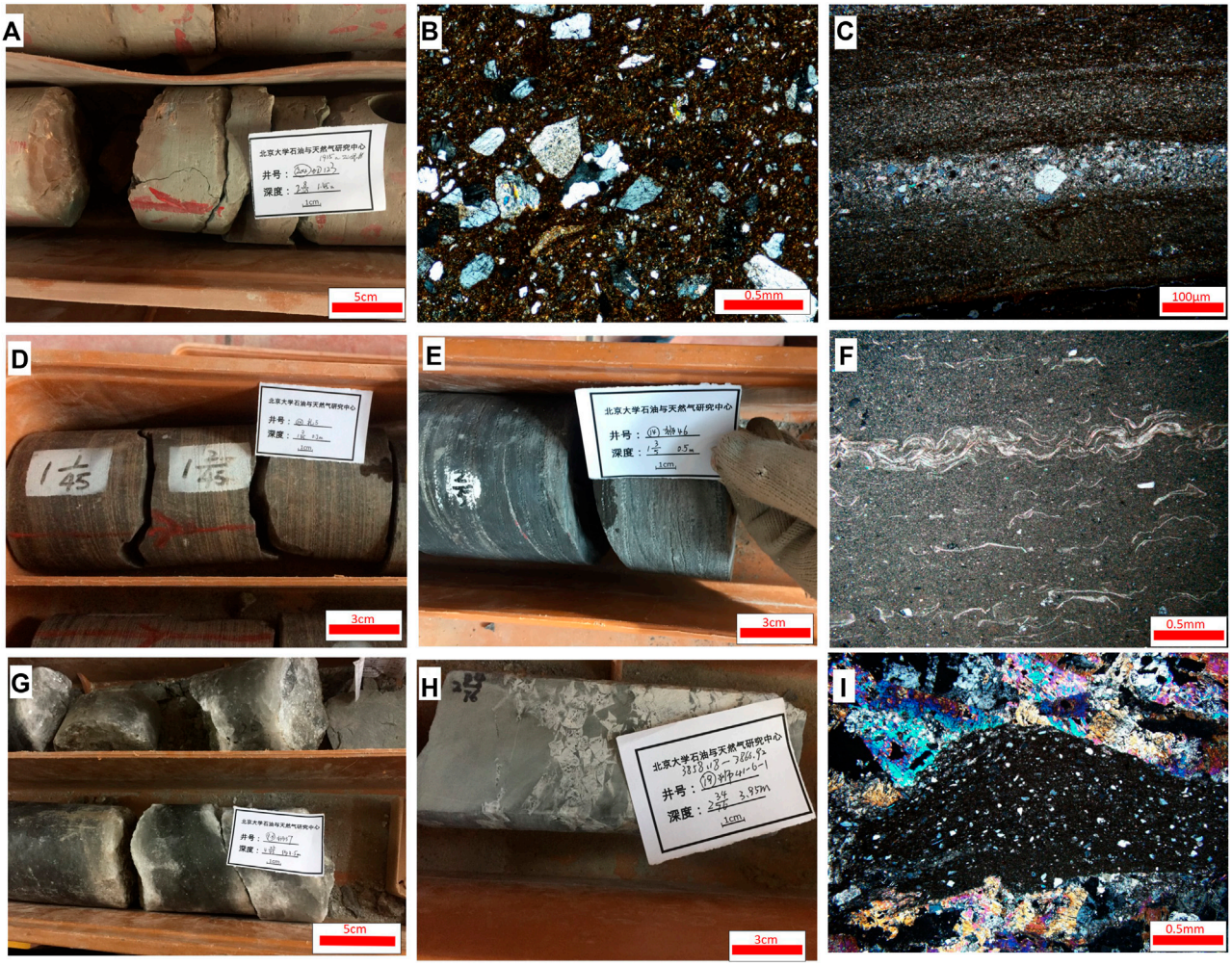

FIGURE 2
Petrographic features of clastic, carbonate, and evaporite rocks **(A)** Brown silty mudstone: sample 204, Well Qie123, 1980.30 m, E_3^1, core; **(B)** Mudstone with dispersed medium and fine sand particles: sample 207, Well Qie 126, 2035.9 m, E_3^1, thin section; **(C)** Calcareous mudstone with horizontal bedding: sample 612, Well Liangzhong 3-3, 1,370.7 m, N_2^2, thin section; **(D)** Micritic limestone with laminated structure: sample 423, Well Zha 5, 3,404 m, N_1, core; **(E)** Relatively homogeneous micritic limestone: sample 315, Well Shi 46, 3,774.9 m, E_3^2, core; **(F)** Micrite limestone with bioturbation structure: sample 406, Well Zha 3, 3,023.54 m, N_1, thin section; **(G)** Halite: sample 308, Well Shi 37, 2,702.1m, E_3^2, core; **(H)** Anhydrite particles dispersed in carbonate matrix: sample 320, Well Shi 41-6-1, 3,862.1 m, E_3^2, core; **(I)** Argillaceous gypsum: sample 317, Well Shi 48, 4,402.1 m, E_3^2, thin section.

The 109 samples were analyzed through X-ray diffraction (XRD), carbon, and oxygen isotopes. The fresh and dense parts without dissolved pores, fissures, and veins were selected for thin slice observation, crushed to less than 200 mesh, and divided into two parts. One part was analyzed using the traditional phosphoric acid method to eliminate the interference of associated dolomite on calcite in the samples (Epstein et al., 1964; Al-Aasm et al., 1990). Sample powders were dissolved in anhydrous phosphoric acid at 25 °C for 40 min and the isotope test was completed on the mat-253 isotope mass spectrometer. Repeated analysis of NBS-19 shows that laboratory precision for both C and O isotope values is <0.2‰(VPDB). The other part was used to analyze the mineral composition of the whole rock via XRD. The two experiments were completed in the National Geological Experiment and Testing Center of the Chinese Academy of Geological Sciences and the Beijing Beidayanyuan Micro Structure Analytical Laboratory, respectively. All the detailed information mentioned above, including location, depth, stratigraphic framework, isotope values, and mineral composition is given in Supplementary Materials.

4 Results

4.1 Lithology and minerals

Among the samples, rocks from the E_3^1 (Eocene) mostly consist of silicate mineralsprimarily composed of quartz and feldspar. The samples from the other four formations are mixed deposits of siliciclastic, carbonate, and evaporite minerals. (Supplementary Table S1; Figure 2). All samples from the five formations can be divided into three major rock types: siliciclastic rocks, carbonate rocks (major part), and evaporite rocks (the mineral content of representative samples revealed by XRD is shown in Figure 3).

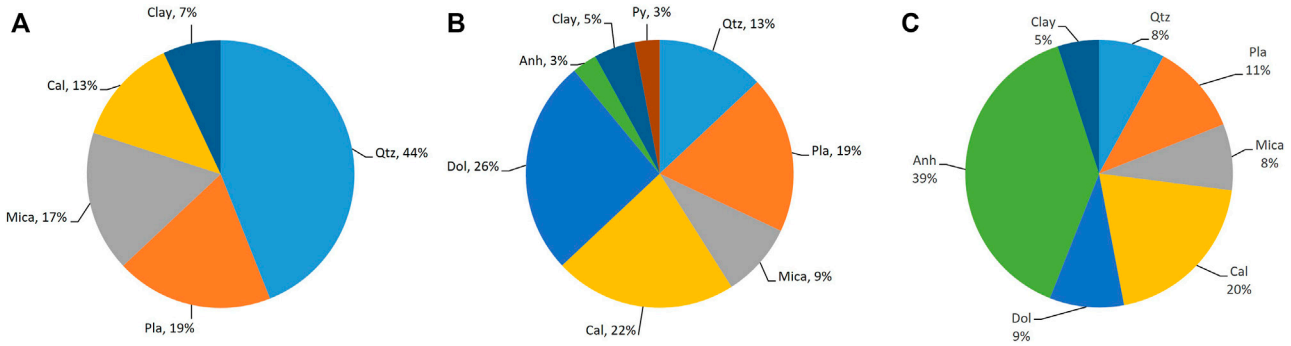

FIGURE 3
The mineral content of representative samples obtained via X-ray diffraction **(A)** is sample 204, Well Qie 123, E_3^1; **(B)** is sample 318, Well Shi 43, E_3^2; **(C)** is sample 317, Well Shi 48, E_3^2).

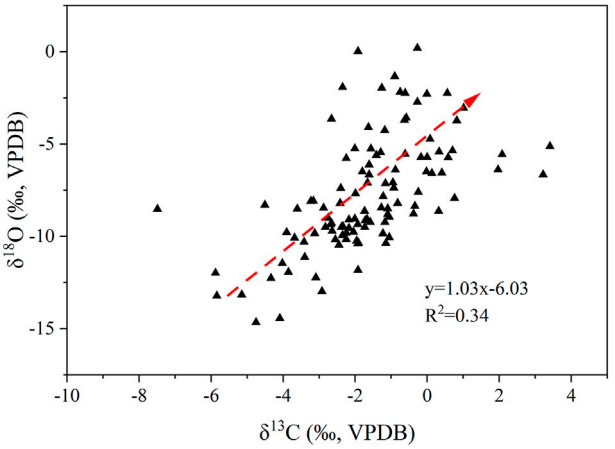

FIGURE 4
Cross plots of C and O isotope.

The siliciclastic rocks are primarily siltstone and argillaceous siltstone (Figures 2A–C). In addition to quartz and feldspar (the main components), they also contain a high content of clay minerals and a low content of carbonate (generally less than 25%) and do not contain anhydrite, halite, or other evaporates (Figure 3A). Carbonates are distributed in the five formations and are the main rock type in the study area (Figures 2D–F). They are primarily micritic limestone or dolomite (Figure 3B), in which the contents of silt, clastic argillite, and evaporite are low (<25%). Evaporites are primarily developed in the E_3^2 (Figures 2G–I); apart from a small number of siliceous clasts and carbonates (Figure 3C), they are predominantly composed of anhydrite (>25%) and a small amount of glauberite and halite (<15%).

4.2 Carbon and oxygen isotopic composition

Isotopic data of calcite is shown in Supplementary Table S1. Samples yield $\delta^{13}C$ values from −7.49‰ to 3.41‰ (average −1.66‰, VPDB) and $\delta^{18}O$ varies of −14.65‰–0.2‰ (average −7.72‰, VPDB). The correlation between the carbon and oxygen isotopes is illustrated in Figure 4, which shows a positive correlation trend.

5 Discussion

5.1 Diagenesis and detrital input analysis

Diagenesis changes the carbon and oxygen isotopic compositions of authigenic carbonate rocks, particularly the oxygen isotopic composition, affecting their representativeness of the environment (De Boever et al., 2017; Ritter et al., 2017). During the sampling process, calcite veins and fissures were avoided where diagenetic alteration and groundwater leaching were inclined to occur; metamorphism, dissolution, and recrystallization were not observed in thin sections (Figure 2). Moreover, most samples were fine-grained rocks (mudstone and some siltstone); thus, they were less likely to be affected by external fluids, acting as tightly structured impermeable layers. The carbon and oxygen isotopes of all samples vary with high frequency over time, with a positive correlation between the isotopes, indicating that the samples were not affected by diagenesis (Garzione et al., 2004; Kent-Corson et al., 2009).

The mixing of extrabasinal detrital carbonate can also affect the representativeness of carbon and oxygen isotopes. Almost all the samples in this study are fine-grained rocks that were deposited after long-distance transportation, during which the carbonate rocks may have broken, dissolved, and hardly preserved. These results are in good agreement with previous studies in the Qaidam Basin (Graham et al., 2005; Kent-Corson et al., 2009; Rieser et al., 2009; Zhuang et al., 2011; Li et al., 2016; Li et al., 2017; Ma et al., 2017; Song et al., 2017). Furthermore, the range of isotope data obtained in this study (Figure 5) is similar to previous results of typical lacustrine carbonates including the Qaidam Basin, further illustrating the reliability of the data.

5.1.1 Data sources

Samples from the E_3^1 to N_2^2 (this study); drilling cores in the western Qaidam Basin (Xiong et al., 2021); the Dahonggou section in the northern margin of Qaidam Basin (Song et al., 2017); the

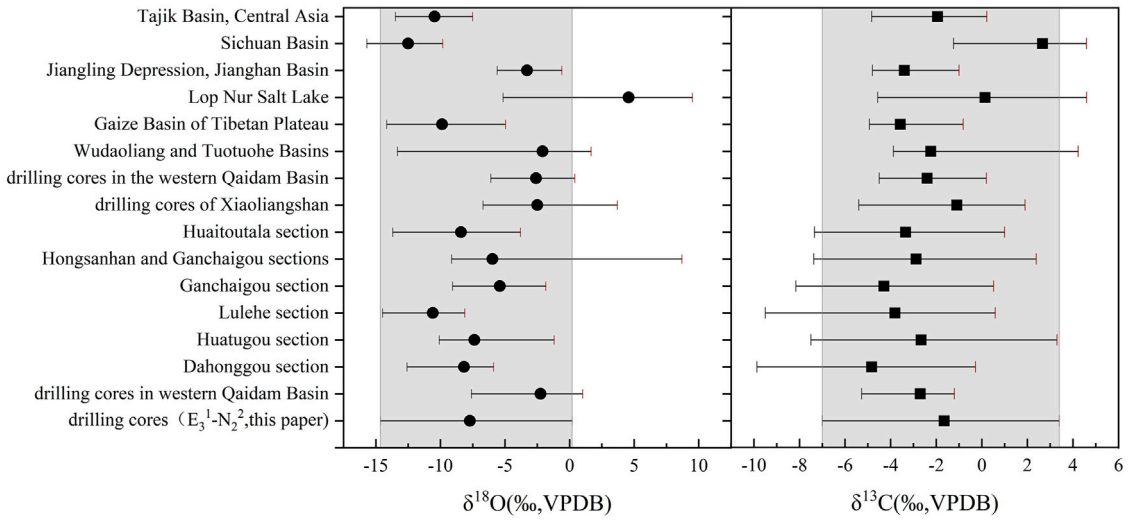

FIGURE 5
Distribution of carbon and oxygen isotopes in salt lakes from different studies.

Huatugou section in the western Qaidam Basin (Li et al., 2016); the Lulehe section in the northern margin of Qaidam Basin (Kent-Corson et al., 2009); the Ganchaigou section in the western Qaidam Basin (Li et al., 2017); the Hongsanhan and Ganchaigou sections in the western Qaidam Basin (Rieser et al., 2009); the Huaitoutala section in the northern margin of Qaidam Basin (Zhuang et al., 2011); drilling cores of Xiaoliangshan in the western Qaidam Basin (Jian et al., 2014); drilling cores in the western Qaidam Basin (Yuan et al., 2015); the Wudaoliang and Tuotuohe Basins of TP (Yi et al., 2007); the Gaize Basin of the TP (Jiang et al., 2016); drilling cores in Lop Nur Salt Lake (Lv et al., 2018); drilling cores in Jiangling Depression, Jianghan Basin (Wang et al., 2013); drilling cores in Sichuan Basin (Zhang et al., 2013); the Tajik Basin, Central Asia (Wang et al., 2020). The location of studies in the Qaidam Basin is illustrated in Figure 1B.

5.2 Isotope controlling factors

The authigenic calcite is considered to crystallize directly from the surface of the lake (Leng and Marshall, 2004). Its carbon and oxygen isotopes, particularly oxygen isotopes, are typically used as good proxies for climate and environmental changes.

The oxygen isotope fractionation during the precipitation of calcite in water is believed to be in line with the equilibrium fractionation process (O'Neil et al., 1969), where the temperature and oxygen isotopes of the water are the major factors controlling oxygen isotope values in the calcite. The temperature has a small effect, approximately 0.24‰/°C (Craig, 1965; Kim and O'Neil, 1997), whereas the role of oxygen isotopes in water is important, including factors such as evaporation and precipitation. For the fractionation of carbon isotopes in calcite precipitation, the temperature has less effect than the oxygen isotope, with a fractionation effect of only 0.035‰/°C (Emrich et al., 1970). The carbon isotope composition of water is most affected by three factors: 1) photosynthesis and respiration of organisms in the lake; 2) CO_2 exchange between lake water and the atmosphere; 3) isotope composition of the injected water (Leng and Marshall, 2004).

The carbon and oxygen isotopes from the Eocene to Oligocene (E_3^1–N_2^2) have a large variation range, 10.9‰ and 14.85‰, respectively. The temperature has little influence on the isotopic fractionation of calcite. If the $\delta^{18}O$ of water had been unchanged, the ambient temperature theoretically must have changed by 61.88°C, which is unlikely in natural deposition processes. Thus, it can be hypothesized that the isotopes of the samples may have been affected by the isotopes of water itself. Furthermore, the carbon and oxygen isotopes and their correlation with the precipitated components (Figure 6) show positive correlation trends. Dolomite and anhydrite in the Qaidam Basin were regarded as the products of water evaporation and condensation (Guo et al., 2017; Xiong et al., 2021), they crystallized and precipitated with continuous growing of the supersaturation, indicating that an increase in precipitated components may represent the evaporation process. It demonstrates that evaporation was the main factor altering the carbon and oxygen isotopes. For the entire basin, the dry or wet climate on a long-term scale was the direct factor controlling evaporation, suggesting that the value of isotopes can reflect the strength of evaporation and the drought or humidity of the climate.

5.3 Paleoclimatic reconstructions

As discussed in Section 5.2, carbon and oxygen isotopes can provide insights into the intensity of evaporation and the wet/dry climate conditions during the Eocene–Miocene (E_3^1–N_2^2). Based on changes in lithology, mineral content, and isotope, three relative drought stages could be identified during this period, as described below (Figure 7).

During Stage Ⅰ (top of E_3^1 to E_3^2, ca.40-32 Ma), the average values of $\delta^{18}O$ and $\delta^{13}C$ in this period are −5.16‰ and −0.88‰,

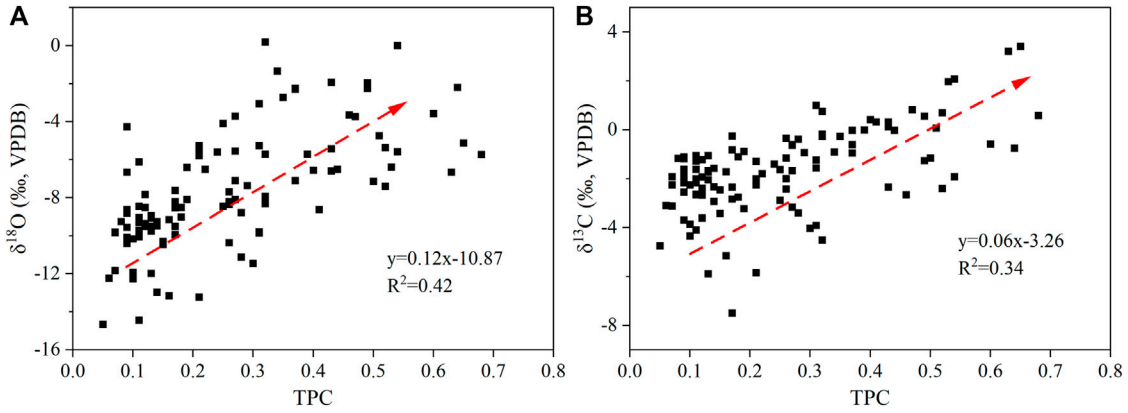

FIGURE 6
Cross plots of Carbon and oxygen isotope data of carbonate components in mixed deposits **(A)** $\delta^{18}O$ versus TPC wt%; **(B)** $\delta^{13}C$ versus TPC wt%. The content of TPC is the sum of calcite, dolomite, anhydrite, glauberite, and halite from the XRD data.

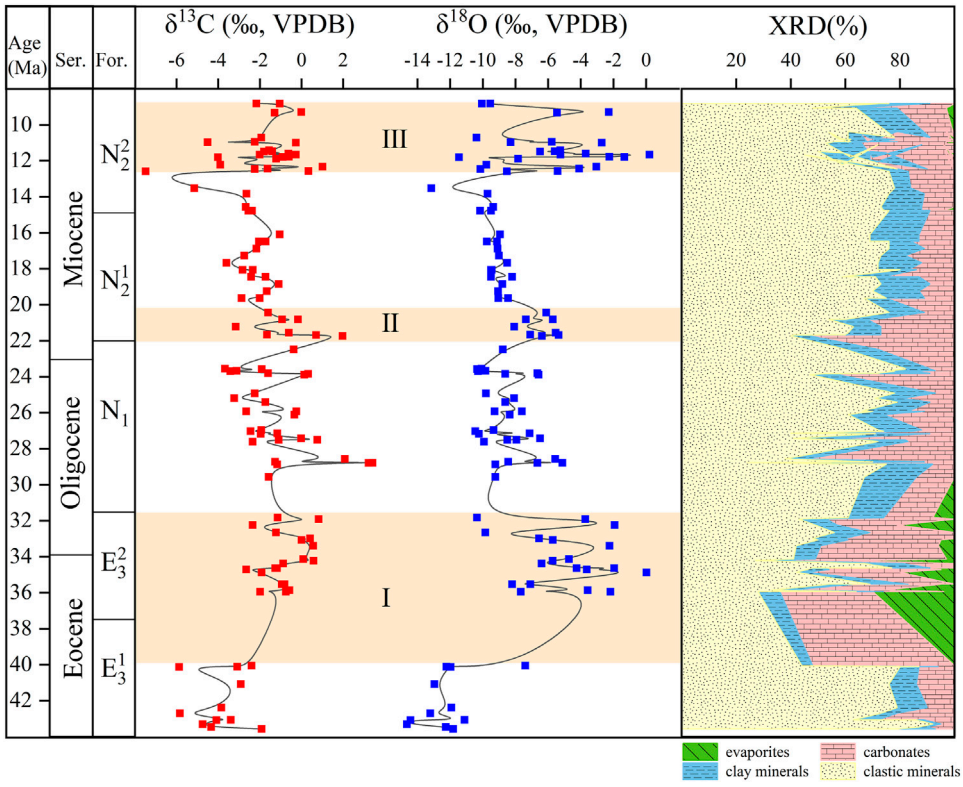

FIGURE 7
Stable isotope values, mineralogy from E_3^1 to N_2^2 in Qaidam Basin. Chronology is based on magnetostratigraphy (Zhang, 2006; Wang et al., 2012; Fang et al., 2019).

respectively, both showing a sharp positive deviation which indicates intense evaporation and drought. The content of siliciclastic components decreases while the average content of carbonate minerals is 31.85%, with dolomite accounting for half. Anhydrite and glauberite are abundant, along with some samples containing halite (Figure 2G), suggesting that the terrigenous detritus was less supplemented at this stage while the evaporation was strong under closed conditions. Pyrite develops in most samples, which further supports the inference of a non-oxidative environment.

During Stage II (bottom of N_2^1, ca.22-20 Ma), the climate variables present relatively high values in comparison with samples of N_1, suggesting a dry climate. The $\delta^{18}O$ and $\delta^{13}C$ have

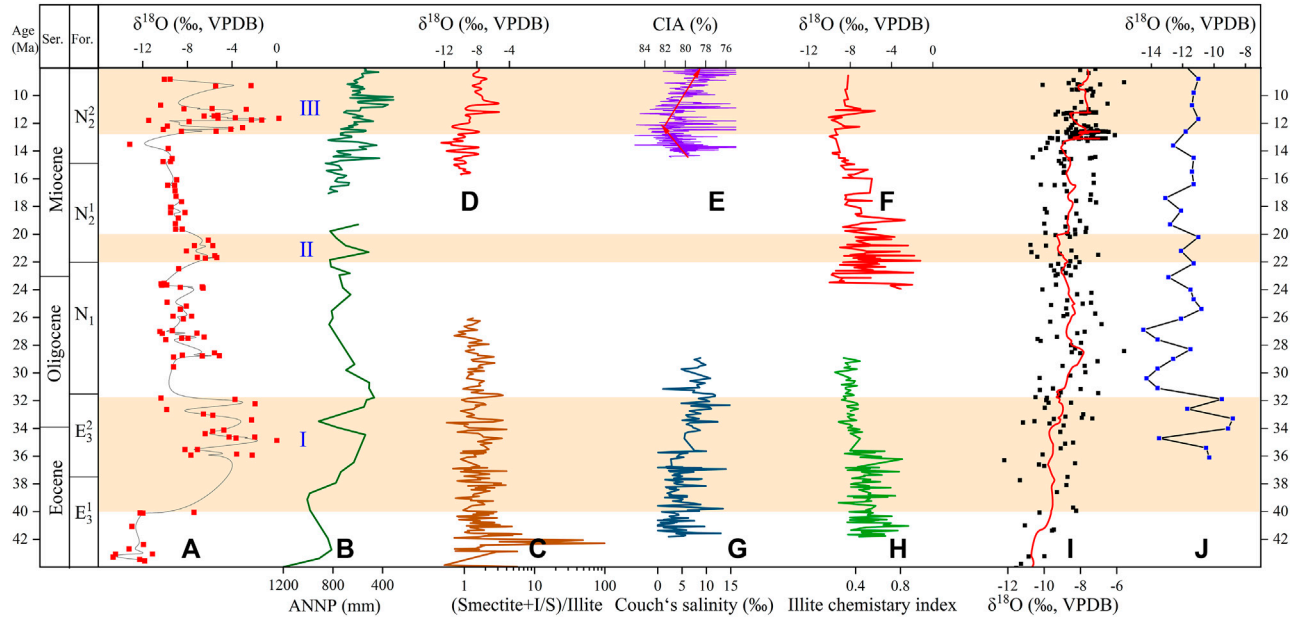

FIGURE 8
Comparisons between the $\delta^{18}O$ values and other climatic indicators from the Qaidam basin. **(A)** the $\delta^{18}O$ values of the western Qaidam Basin (this study); **(B)** mean annual precipitation (ANNP) of the Qaidam Basin (Jia et al., 2021); **(C,G,H)** (Smectite + I/S)/illite ratios, couch's salinity and illite chemistry index in the Hongliugou (HLG) section (Fang et al., 2019; Ye et al., 2020); **(D,E)** Carbonate $\delta^{18}O$ and CIA record in the Huaitoutala (HTTL) section (Zhuang et al., 2011; Bao et al., 2019); **(F)** Carbonate $\delta^{18}O$ record in the Huatugou (HTG) section (Li et al., 2016); **(I)** Carbonate $\delta^{18}O$ record in the Dahonggou (DHG) section (Sun et al., 2020); **(J)** Carbonate $\delta^{18}O$ record in the Lulehe (LLH) section (Kent-Corson et al., 2009). The location of the aforementioned sections within the basin is illustrated in Figure 1A.

a large positive deviation, ranging from an average of −8.48‰ and −1.06‰ in N_1 to −6.46‰ and −0.68‰, respectively. The carbonate mineral content slightly increases (up to 53%, with an average of 32.25‰). Nevertheless, this arid climate did not last for an extended period of time.

During Stage III (top of N_2^2, ca.13-8.2 Ma), the climate is characterized by persistent drought like Stage I, with $\delta^{18}O$ and $\delta^{13}C$ are −6.02‰ and −1.74‰, respectively. Furthermore, the XRD results reveal that the content of siliciclastic minerals decreases, while dolomite increases substantially. Besides, evaporates such as halite are also observed.

The above three dry stages are well recorded in many sections. The Stage I revealed by $\delta^{18}O$ values and minerals content (Figure 8A) is well reflected in the Qaidam Basin: e.g., the distinct decrease of CIA ratios, (Smectite+I/S)/illite ratios (Figure 8C) and illite chemistry index (Figure 8H), and the increase of paleosalinity (Figure 8G) at ~40 Ma (Song et al., 2013; Ye et al., 2016; Fang et al., 2019; Ye et al., 2020). The multi-method-based mean annual precipitation (ANNP) derived from four pollen records (core SG-1, SG-1b, KC-1, and DHG section) indicates a persistent decreasing trend during this period (Figure 8B) (Jia et al., 2021). The short-time dry Stage II has also been recorded: the positive bias of $\delta^{13}C$ and $\delta^{18}O$ in the Ganchaigou and HTG sections (Figure 8F) (Li et al., 2016; Li et al., 2017), and the abrupt decrease of ANNP at ~22 Ma (Figure 8B) (Jia et al., 2021). The Stage III is broadly consistent with the decline of ANNP since ~14 Ma (Figure 8B) (Jia et al., 2021) and the increase of carbonate $\delta^{18}O$ after ~13 Ma of the DHG section (Figure 8I) (Sun et al., 2020). The carbonate $\delta^{18}O$ of the HTTL section (Figure 8D) (Zhuang et al., 2011), HTG section (Figure 8F) (Li et al., 2016), LLH section (Figure 8J) (Kent-Corson et al., 2009) and the CIA ratios of the HTTL section (Figure 8E) (Bao et al., 2019) also exhibit a trend of continuous increase. Total organic carbon (TOC), mineralogy, leaf wax alkanes, and plant sporopollen studies conducted in the Honggouzi and Qigequan sections as well as drilling cores have all confirmed the occurrence of this event (Wang et al., 1999; Song et al., 2014; Miao et al., 2016; Wu et al., 2019). The timings of the various sections exhibited variability, yet they remained within a narrow range (which may also be subject to chronological imprecision).

5.4 Drivering mechanisms of aridification

Several main drivers of the aridification in the northern TP have been proposed: global cooling (Dupont-Nivet et al., 2007; Li et al., 2018; Page et al., 2019), the uplift of the TP and the margins (Caves, 2017; Wang et al., 2020), Paratethys Sea regression (Ramstein et al., 1997; Bougeois et al., 2018; Fang et al., 2019), pCO_2 concentrations (Bond and Midgley, 2012; Fang et al., 2019), and the combined factors.

Global climate can affect vapor transport efficiency and global sea-level change (Li et al., 2018). The persistent global cooling during the Cenozoic has weakened the hydrological cycle (Herbert et al., 2016) and lowered the sea level (Miller et al., 2020), contributing to the arid climate in the continental interior. The distinct increase of $\delta^{18}O$ values together with the decrease of ANNP (Jia et al., 2021) in

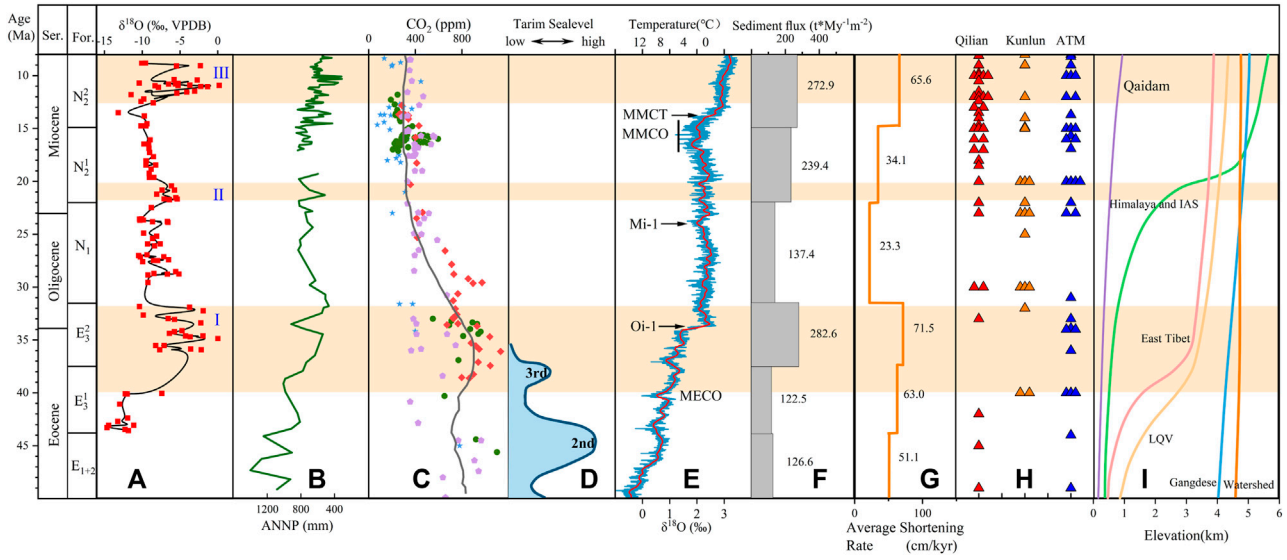

FIGURE 9
Comparisons between the $\delta^{18}O$ values of the Qaidam Basin with other records. **(A)** the $\delta^{18}O$ values of the western Qaidam Basin (this study); **(B)** the mean annual precipitation (ANNP) of the Qaidam Basin (Jia et al., 2021); **(C)** multi-proxy atmospheric CO_2 (Foster et al., 2017) (red: $\delta^{13}C$ of alkenones; green: boron isotopes; purple: leaf stomata; blue: $\delta^{13}C$ of paleosols); **(D)** the approximate relative changes in sea levels in the TB during each sea transgression/regression (Bosboom et al., 2014a; Bosboom et al., 2014b); **(E)** global benthic foraminiferal $\delta^{18}O$ stack (Westerhold et al., 2020); **(F)** sedimentary flux and **(G)** average shortening rate for the QB (Bao et al., 2017); **(H)** tectonic events in the Qilian Mountains, Kunlun Fault, and Altyn-Tagh Mountains, respectively. Each triangle represents a tectonic event, which includes the onset of thrust faulting, apatite fission track cooling ages, (U-Th)/He ages and thermal models from the northern TP, and others. Data and references are supplied in Supplementary Table S2. **(I)** Paleo-elevation reconstructions of the TP including the Qaidam Basin (Ding et al., 2022; Wu et al., 2022).

Stage III highly correlated with the global cooling reflected by increasing benthic foraminiferal $\delta^{18}O$ (Figure 9E) (Westerhold et al., 2020). Given the favorable correspondence of the starting time, the global cooling may be the main driver for the aridity in the northern TP since 13 Ma. However, there is no obvious variation of benthic foraminiferal $\delta^{18}O$ during the Stages I and II. This inconsistency highlights the complexity of drivers and suggests that global cooling alone may not be sufficient to explain the aridity in the Qaidam Basin.

The TP (location shown in Figure 1A), the highest plateau in the world, exerts a complex and profound influence on climate change. High-resolution general circulation models have projected the uplift of the TP has led to aridification of the Aisan interior, via orographic blocking of moist air from the Indian Ocean, and by forcing the westerlies to flow around the northern rim of the TP (Kutzbach et al., 1989; Ruddiman and Kutzbach, 1989; Manabe and Broccoli, 1990). Furthermore, the plateau is not a monolithic entity but rather comprises multiple terranes that have undergone distinct uplift histories (Ding et al., 2022; Xiong et al., 2022). Quantitative paleoaltimetry studies (stable isotopes, clumped isotope, ecological methods) in Lhasa-Qiangtang suture valley (LQV) and Eastern Tibet, including Nangqian (Li et al., 2018), Gonjo (Xiong et al., 2020) and Lunpola (Rowley and Currie, 2006; Ingalls et al., 2020) basins, suggest that they almost reached 2000m by 40 Ma and experienced a sharp uplift during the Stage I (Figure 9I). Moreover, tectonic investigations (sedimentology, thermochronology and so on) have revealed the early exhumation of the Qilian, Kunlun, and Altyn-Tagh Mountains in the northern TP (Figure 9H) (e.g., Wang et al., 2016; Liu et al., 2017; He et al., 2018) since late Eocene, and the sediment flux and average shortening rate of the basin also increased (Figures 9F, G) (Bao et al., 2017). The aridity since ~40 Ma may be controlled by the above uplifts and exhumations rather than global cooling.

As for stage II and III, the tectonic evolution may have also played a role in the climatic change observed. The above three mountains surrounding the Qaidam Basin underwent extensive rapid cooling during the early-middle Miocene (Figure 9H) (e.g., Lease et al., 2011; Cheng et al., 2016; Wu et al., 2021), accompanied with the large sediment flux and basin average shortening rate (Figures 9F, G) (Bao et al., 2017). During stage II the global temperature remains relatively stable, similar to stage I. Therefore, we attribute the main cause of aridity to the uplift of mountains around the basin. During the stage III, the tectonic events in the surrounding orogenic belts entered in a very active stage (Figure 9H). For example, the South Qilian Shan experienced a rapid exhumation since ~14 Ma (Li et al., 2020b; Fu et al., 2022). Therefore, we believe that both the tectonic evolution causing by uplift of the TP and the global cooling were responsible for inducing the aridity of stage III.Climate modeling and proxies suggest that central Asia has been governed by the westerly moisture of the Paratethys Sea (Caves et al., 2015; Wang et al., 2020), which extended Eurasia as far as the TB (Figure 1A). Three Paleogene sea transgressions and regressions have been previously identified, and Bosboom et al. (2014a), Bosboom et al., 2014b, Bosboom et al. (2018) found that the second westward regression of the Paratetythys Sea started at ~41 Ma and the final regression from the TB occurred prior to ~34 Ma (Figure 9D). The distinct aridity indicated by $\delta^{18}O$ and ANNP records of the Qaidam Basin since

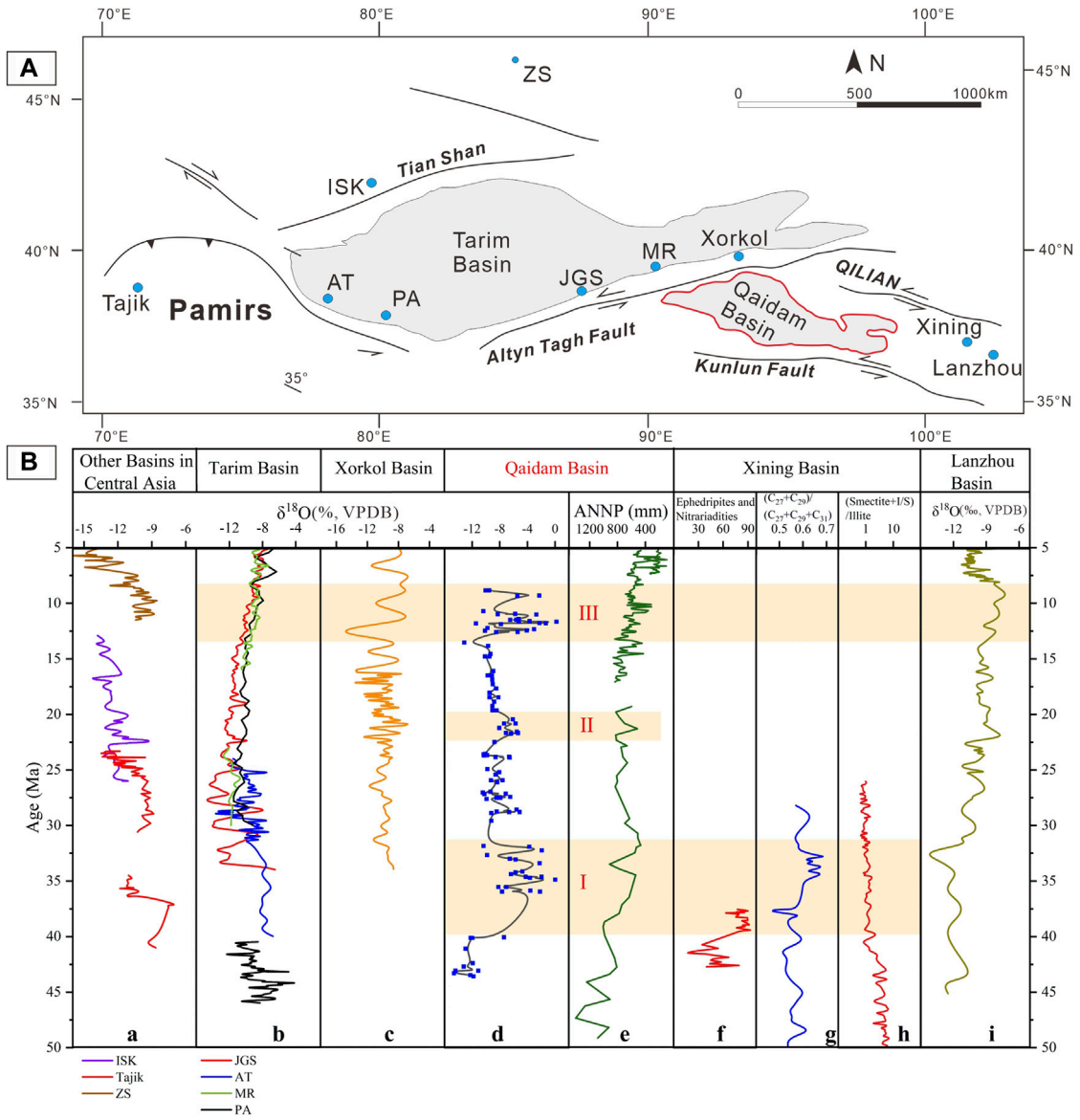

FIGURE 10
(A) Location of climatic studies in Central Asia. **(B)** $\delta^{18}O$ data from the Qaidam Basin and other published records from the Central Aisa. **(a–d)** the $\delta^{18}O$ values from ISK—Issyk Kul (Macaulay et al., 2016), Tajik (Wang et al., 2020), ZS—Zysan (Caves, 2017); Tarim Basin: JGS-Janggalsay, AT-Aertashi, PA-Puska, MR-Miran River (Kent-Corson et al., 2009); Xorkol Basin (Kent-Corson et al., 2009); western Qaidam Basin (this study); **(e)** mean annual precipitation (ANNP) of the Qaidam Basin (Jia et al., 2021); **(f–h)** Xining Basin (XB): Ephedripites and Nitrariadities in pollen records (Bosboom et al., 2014c), $(C_{27}+C_{29})/(C_{27}+C_{29}+C_{31})$ of n-Alkanes (Long et al., 2011); (Smectite + I/S)/illite ratios (Fang et al., 2019); **(i)** the $\delta^{18}O$ values from Lanzhou Basin (LB) (Li et al., 2016).

~40 Ma is roughly contemporaneous with the time of regression (Figures 9A, B, D), which may have resulted in a reduction in moisture supply from the sea eastward into the Qaidam Basin (Kaya et al., 2019; Meijer et al., 2019). The drivers behind the regressions are multifaceted, encompassing far-field tectonic effects of the India-Aisa collision, early Pamir/Tibetan activation, as well as long-time sea level fluctuations (Bosboom et al., 2014a; Kaya et al., 2019). Therefore, we consider that the Paratethys plays a crucial role in shaping the stage I aridity of the Qaidam Basin along with the uplift of the TP.

The increase in atmospheric pCO_2 could increase mean global temperature, thereby affecting atmospheric and oceanic circulation, precipitation patterns, and intensity (Zachos and Kump, 2005; Zachos et al., 2008). It can also influence the aridity through the vegetation-physiological forcing, e.g., tress-grass competition (Bond and Midgley, 2012). However, the increase of $\delta^{18}O$ at~40 Ma was earlier than the pCO_2 drop during the Oligocene period (Figure 9C). And the other two aridity events were also inconsistent with the relatively stable pCO_2 since the Early Miocene (Foster et al., 2017). Compared to the global temperature recorded by $\delta^{18}O$, the data

sources of atmospheric pCO_2 are more dispersed with a larger error range (Figure 9C). Given the above reasons, we suggest that the pCO_2 may have played a limited role in the aridification in the Qaidam Basin and need to be studied further.

To investigate the climatic evolution relationship between the Qaidam Basin and other surrounding basins, we have compiled the regional paleoclimatic proxy studies from a vast area spanning from Tajik Basin in the west to LB in the east (Figure 10). The distinct increase of $\delta^{18}O$ and the ANNP records of the Qaidam Basin during the Stage Ⅰ is consistent with the aridity observed in XB, as evidenced by Ephedripites and Nitrariadities in pollen records (Figure 10f) (Bosboom et al., 2014c), $(C_{27}+C_{29})/(C_{27}+C_{29}+C_{31})$ of n-Alkanes (Figure 10g) (Long et al., 2011) and (Smectite + I/S)/illite ratios (Figure 10h) (Fang et al., 2019). In contrast, the isotopic records from the LB, the TB, and other western basins remain relatively stable without significant changes during this period (Figures 10a, b, i). The aridity of Stage Ⅰ in the Qaidam Basin may be attributed to the regression of the Paratethys Sea and the uplift of the TP, which could also have impacted the adjacent XB (Bosboom et al., 2014c; Fang et al., 2019; Meijer et al., 2019). During this stage, the climate in the LB may have been influenced by the East Asian summer monsoon rather than westerlies, and the LB is located within the transitional zone between the Chinese Loess Plateau and the TP at present. Besides, the contrast implies that the TB and other basins in Central Aisan have experienced less impact from the regression due to their relatively closer proximity to the sea compared to the eastern basins. The mechanisms behind the above contrast are only speculative, and we highlight that the inconsistencies call for a comprehensive collaboration for understanding the interactions between paleohydrology, paleoecology, and numerical modeling.

The aridity during ca.22-20 Ma in the Qaidam Basin appears to be a localized event, as no corresponding response was observed in other basins. However, the distinct drought since ca.~13 Ma was well-documented in many basins, including the TB to the west and the LB to the east (Figures 10b–i), with the exceptions such as Tajik Basin (Figure 10a). Although there is a lack of climatic record in the XB during this period, it is probable that the same transition occurred within it. This implies that the observed changes since ca.~13 Ma are a regional event controlled by the global cooling rather than a local one (Zhuang et al., 2011; Wu et al., 2022), as also evidenced by their presence in Linxia Basin (Dettman et al., 2003). The continuous decrease of $\delta^{18}O$ in the Tajik Basin and other western basins, located windward of the Pamir-Tian Shan mountains, began as early as ca.~25 Ma (Figure 10a). This significant contrast is likely related to the uplift of Pamir-Tian Shan mountain range, which acted as a moisture barrier for the westerlies since ca.~25 Ma (Caves, 2017; Wang et al., 2020).

6 Conclusion

This study presents a detailed mineralogical, carbon, and oxygen isotope geochemical investigation of Cenozoic sediments in the western Qaidam Basin. There is a noticeable correlation between isotopes and precipitated mineral contents. Through the above mineralogical and isotopic analyses, three aridity stages can be identified during the Eocene to the Miocene (ca.43.8–8.2 Ma): top of E_3^1 to E_3^2 (ca.40-32 Ma), bottom of N_2^1 (ca.22-20 Ma), top of N_2^2 (ca.13-8.2 Ma). Through the comparison of Cenozoic global climatic evolution and tectonic history related to the India–Eurasia collision, it is suggested that stage Ⅰ aridity may have been linked to the regression of the Paratethys Sea and uplift of the TP, the Stage Ⅱ aridity could have resulted from by the mountains uplift and denudation of the around the Qaidam Basin, and Stage Ⅲ aridity might be attributed to global cooling and tectonic events in the northern TP. By comparing the climate records of the Qaidam Basin with those of other basins in Central Asia, stage Ⅰ and Ⅲ aridity may represent two regional climatic events, while Stage Ⅱ aridity appears to be confined to the interior of Qaidam Basin.

Data availability statement

The datasets presented in this study can be found in online repositories. The names of the repository/repositories and accession number(s) can be found in the article/Supplementary Material.

Author contributions

Formal analysis, writing-original draft preparation, SL; methodology, formal analysis, PL; writing—review and editing, project administration, PG; resources, DZ and XX; data processing, XD and JZ; visualization, CZ and JT; All authors contributed to the article and approved the submitted version.

Funding

This research was funded by the National Key R&D Program of China, Grant Number: 2021YFA0719000, and the National Nature Science Foundation of China, Grant Number: 42141021.

Conflict of interest

Authors DZ and XX were employed by Qinghai Oilfield Company, PetroChina.

The remaining authors declare that the research was conducted in the absence of any commercial or financial relationships that could be construed as a potential conflict of interest.

Publisher's note

Supplementary material

The Supplementary Material for this article can be found online at: https://www.frontiersin.org/articles/10.3389/feart.2023.1217304/full#supplementary-material

References

Al-Aasm, I. S., Taylor, B. E., and South, B. (1990). Stable isotope analysis of multiple carbonate samples using selective acid extraction. *Chem. Geol. Isot. Geosci. Sect.* 80, 119–125. doi:10.1016/0168-9622(90)90020-D

Bao, J., Song, C., Yang, Y., Fang, X., Meng, Q., Feng, Y., et al. (2019). Reduced chemical weathering intensity in the Qaidam Basin (NE Tibetan plateau) during the late cenozoic. *J. Asian Earth Sci.* 170, 155–165. doi:10.1016/j.jseaes.2018.10.018

Bao, J., Wang, Y., Song, C., Feng, Y., Hu, C., Zhong, S., et al. (2017). Cenozoic sediment flux in the Qaidam Basin, northern Tibetan Plateau, and implications with regional tectonics and climate. *Glob. Planet. Change* 155, 56–69. doi:10.1016/j.gloplacha.2017.03.006

Benavente, C. A., Mancuso, A. C., and Bohacs, K. M. (2019). Paleohydrogeologic reconstruction of Triassic carbonate paleolakes from stable isotopes: Encompassing two lacustrine models. *J. South Am. Earth Sci.* 95, 102292. doi:10.1016/j.jsames.2019.102292

Bond, W. J., and Midgley, G. F. (2012). Carbon dioxide and the uneasy interactions of trees and savannah grasses. *Philosophical Trans. R. Soc. B Biol. Sci.* 367, 601–612. doi:10.1098/rstb.2011.0182

Bosboom, R., Abels, H. A., Hoorn, C., van den Berg, B. C. J., Guo, Z., and Dupont-Nivet, G. (2014c). Aridification in continental Asia after the middle Eocene climatic optimum (MECO). *Earth Planet. Sci. Lett.* 389, 34–42. doi:10.1016/j.epsl.2013.12.014

Bosboom, R., Dupont-Nivet, G., Grothe, A., Brinkhuis, H., Villa, G., Mandic, O., et al. (2014b). Linking Tarim Basin sea retreat (west China) and Asian aridification in the late Eocene. *Basin Res.* 26, 621–640. doi:10.1111/bre.12054

Bosboom, R., Dupont-Nivet, G., Grothe, A., Brinkhuis, H., Villa, G., Mandic, O., et al. (2014a). Timing, cause and impact of the late Eocene stepwise sea retreat from the Tarim Basin (west China). *Palaeogeogr. Palaeoclimatol. Palaeoecol.* 403, 101–118. doi:10.1016/j.palaeo.2014.03.035

Bougeois, L., Dupont-Nivet, G., de Rafélis, M., Tindall, J. C., Proust, J., Reichart, G., et al. (2018). Asian monsoons and aridification response to Paleogene sea retreat and Neogene westerly shielding indicated by seasonality in Paratethys oysters. *Earth Planet. Sci. Lett.* 485, 99–110. doi:10.1016/j.epsl.2017.12.036

Bristow, T. F., Kennedy, M. J., Morrison, K. D., and Mrofka, D. D. (2012). The influence of authigenic clay formation on the mineralogy and stable isotopic record of lacustrine carbonates. *Geochim. Cosmochim. Acta* 90, 64–82. doi:10.1016/j.gca.2012.05.006

Caves, J. K. (2017). Late Miocene uplift of the tian Shan and altai and reorganization of central Asia climate. *GSA Today* 27, 19–26. doi:10.1130/GSATG305A.1

Caves, J. K., Sjostrom, D. J., Mix, H. T., Winnick, M. J., and Chamberlain, C. P. (2014). Aridification of central Asia and uplift of the altai and hangay mountains, Mongolia: Stable isotope evidence. *Am. J. Sci.* 314, 1171–1201. doi:10.2475/08.2014.01

Caves, J. K., Winnick, M. J., Graham, S. A., Sjostrom, D. J., Mulch, A., and Chamberlain, C. P. (2015). Role of the westerlies in central Asia climate over the cenozoic. *Earth Planet. Sci. Lett.* 428, 33–43. doi:10.1016/j.epsl.2015.07.023

Cheng, F., Fu, S. T., Jolivet, M., Zhang, C. H., and Guo, Z. J. (2016). Source to sink relation between the eastern Kunlun range and the Qaidam Basin, northern Tibetan plateau, during the cenozoic. *Geol. Soc. Am. Bull.* 128, 312601–313283. doi:10.1130/B31260.1

Cheng, F., Jolivet, M., Guo, Z., Wang, L., Zhang, C., and Li, X. (2021). Cenozoic evolution of the Qaidam basin and implications for the growth of the northern Tibetan plateau: A review. *Earth-Sci. Rev.* 220, 103730. doi:10.1016/j.earscirev.2021.103730

Craig, H. (1965). "The measurement of oxygen isotope paleotemperatures," in *Stable Isotopes in Oceanographic Studies and Palaeotemperatures*. Editor E. Tongiorgi (Pisa: Consiglio Nazionale delle Ricerche Laboratorio di Geologia Nucleare), 161–182.

Dai, S., Fang, X., Dupont-Nivet, G., Song, C., Gao, J., Krijgsman, W., et al. (2006). Magnetostratigraphy of cenozoic sediments from the Xining Basin: Tectonic implications for the northeastern Tibetan plateau. *J. Geophys. Res. Solid Earth* 111, n/a. doi:10.1029/2005JB004187

De Boever, E., Brasier, A. T., Foubert, A., and Kele, S. (2017). What do we really know about early diagenesis of non-marine carbonates? *Sediment. Geol.* 361, 25–51. doi:10.1016/j.sedgeo.2017.09.011

Dettman, D. L., Fang, X., Garzione, C. N., and Li, J. (2003). Uplift-driven climate change at 12 Ma: A long δ18O record from the NE margin of the Tibetan plateau. *Earth Planet. Sci. Lett.* 214, 267–277. doi:10.1016/S0012-821X(03)00383-2

Ding, L., Kapp, P., Cai, F., Garzione, C. N., Xiong, Z., Wang, H., et al. (2022). Timing and mechanisms of Tibetan Plateau uplift. *Nat. Rev. Earth Environ.* 3, 652–667. doi:10.1038/s43017-022-00318-4

Dupont-Nivet, G., Hoorn, C., and Konert, M. (2008). Tibetan uplift prior to the Eocene-Oligocene climate transition: Evidence from pollen analysis of the Xining Basin. *Geology* 36, 987. doi:10.1130/G25063A.1

Dupont-Nivet, G., Krijgsman, W., Langereis, C. G., Abels, H. A., Dai, S., and Fang, X. (2007). Tibetan plateau aridification linked to global cooling at the Eocene–Oligocene transition. *Nature* 445, 635–638. doi:10.1038/nature05516

Emrich, K., Ehhalt, D. H., and Vogel, J. C. (1970). Carbon isotope fractionation during the precipitation of calcium carbonate. *Earth Planet. Sci. Lett.* 8, 363–371. doi:10.1016/0012-821X(70)90109-3

Epstein, S., Graf, D. L., and Degens, E. T. (1964). "Oxygen isotope studies on the origin of dolomites," in *Isotopic and cosmic chemistry* (Amsterdam: North Holland), 169–180.

Fang, X., Galy, A., Yang, Y., Zhang, W., Ye, C., and Song, C. (2019a). Paleogene global cooling–induced temperature feedback on chemical weathering, as recorded in the northern Tibetan Plateau. *Geology* 47, 992–996. doi:10.1130/G46422.1

Fang, X., Zhang, W., Meng, Q., Gao, J., Wang, X., King, J., et al. (2007). High-resolution magnetostratigraphy of the neogene Huaitoutala section in the eastern Qaidam Basin on the NE Tibetan plateau, Qinghai province, China and its implication on tectonic uplift of the NE Tibetan plateau. *Earth Planet. Sci. Lett.* 258, 293–306. doi:10.1016/j.epsl.2007.03.042

Fang, Y., Fang, X., Zan, J., Zhang, T., Yang, Y., Ye, C., et al. (2019b). An Asian inland aridification enhancement event at ~39 Ma recorded by total organic carbon isotopes from Xining Basin. *J. Earth Environ.* 10, 453–464.

Foster, G. L., Royer, D. L., and Lunt, D. J. (2017). Future climate forcing potentially without precedent in the last 420 million years. *Nat. Commun.* 8, 14845. doi:10.1038/ncomms14845

Fu, H., Jian, X., Liang, H., Zhang, W., Shen, X., and Wang, L. (2022). Tectonic and climatic forcing of chemical weathering intensity in the northeastern Tibetan Plateau since the middle Miocene. *Catena* 208, 105785. doi:10.1016/j.catena.2021.105785

Fu, L., Ping, G., Xing, J., Ruijuan, L., Fan, F., Qun, A., et al. (2012). Sedimentary genetic types of coarse fragment of paleogene Lulehe formation in Qaidam Basin and time limit of the Tibetan plateau uplift. *Nat. Gas. Geosci.* 23, 833–840.

Garzione, C. N., Dettman, D. L., and Horton, B. K. (2004). Carbonate oxygen isotope paleoaltimetry: Evaluating the effect of diagenesis on paleoelevation estimates for the Tibetan plateau. *Palaeogeogr. Palaeoclimatol. Palaeoecol.* 212, 119–140. doi:10.1016/s0031-0182(04)00307-4

Graham, S. A., Chamberlain, C. P., Yue, Y. J., Ritts, B. D., Hanson, A. D., Horton, T. W., et al. (2005). Stable isotope records of Cenozoic climate and topography, Tibetan plateau and Tarim basin. *Am. J. Sci.* 305, 101–118. doi:10.2475/ajs.305.2.101

Guan, P., and Jian, X. (2013). The Cenozoic sedimentary record in Qaidam Basin and its implications for tectonic evolution of northern Tibetan Plateau. *Acta Sedimentol. Sin.* 31, 824–833.

Guo, P., Liu, C., Huang, L., Wang, P., Wang, K., Yuan, H., et al. (2017). Genesis of the late Eocene bedded halite in the Qaidam Basin and its implication for paleoclimate in east Asia. *Palaeogeogr. Palaeoclimatol. Palaeoecol.* 487, 364–380. doi:10.1016/j.palaeo.2017.09.023

Guo, Z. T., Sun, B., Zhang, Z. S., Peng, S. Z., Xiao, G. Q., Ge, J. Y., et al. (2008). A major reorganization of Asian climate by the early Miocene. *Clim. Past.* 4, 153–174. doi:10.5194/cp-4-153-2008

Harrison, T. M., Copeland, P., Kidd, W., and Yin, A. N. (1992). Raising Tibet. *Science* 255, 1663–1670. doi:10.1126/science.255.5052.1663

He, P., Song, C., Wang, Y., Meng, Q., Chen, L., Yao, L., et al. (2018). Cenozoic deformation history of the Qilian Shan (northeastern Tibetan Plateau) constrained by detrital apatite fission-track thermochronology in the northeastern Qaidam Basin. *Tectonophysics* 749, 1–11. doi:10.1016/j.tecto.2018.10.017

Herbert, T. D., Lawrence, K. T., Tzanova, A., Peterson, L. C., Caballero-Gill, R., and Kelly, C. S. (2016). Late Miocene global cooling and the rise of modern ecosystems. *Nat. Geosci.* 9, 843–847. doi:10.1038/ngeo2813

Hough, B. G., Garzione, C. N., Wang Zhicai, W. Z., Lease, R. O., Burbank, D. W., and Yuan Daoyang, Y. D. (2011). Stable isotope evidence for topographic growth and basin segmentation; implications for the evolution of the NE Tibetan Plateau. *Geol. Soc. Am. Bull.* 123, 168–185. doi:10.1130/B30090.1

Ingalls, M., Rowley, D. B., Currie, B. S., and Colman, A. S. (2020). Reconsidering the uplift history and peneplanation of the northern Lhasa terrane, Tibet. *Am. J. Sci.* 320, 479–532. doi:10.2475/06.2020.01

Ji, J., Zhang, K., Clift, P. D., Zhuang, G., Song, B., Ke, X., et al. (2017). High-resolution magnetostratigraphic study of the paleogene-neogene strata in the northern Qaidam Basin: Implications for the growth of the northeastern Tibetan plateau. *Gondwana Res.* 46, 141–155. doi:10.1016/j.gr.2017.02.015

Jia, Y., Wu, H., Zhang, W., Li, Q., Yu, Y., Zhang, C., et al. (2021). Quantitative Cenozoic climatic reconstruction and its implications for aridification of the northeastern Tibetan Plateau. *Palaeogeogr. Palaeoclimatol. Palaeoecol.* 567, 110244. doi:10.1016/j.palaeo.2021.110244

Jian, X., Guan, P., Fu, S., Zhang, D., Zhang, W., and Zhang, Y. (2014). Miocene sedimentary environment and climate change in the northwestern Qaidam basin, northeastern Tibetan Plateau: Facies, biomarker and stable isotopic evidences. *Palaeogeogr. Palaeoclimatol. Palaeoecol.* 414, 320–331. doi:10.1016/j.palaeo.2014.09.011

Jian, X., Guan, P., Zhang, W., and Feng, F. (2013). Geochemistry of Mesozoic and Cenozoic sediments in the northern Qaidam basin, northeastern Tibetan Plateau:

Implications for provenance and weathering. *Chem. Geol.* 360-361, 74–88. doi:10.1016/j.chemgeo.2013.10.011

Jiang, G., Yadong, X. U., Song, B., Zhang, K., and Luo, L. (2016). The late Eocene aridification of Tibetan plateau:evidence from carbon and oxygen isotopes of kangtuo foramtion primary carbonates in Gaize Basin. *Acta Geol. Sin.* 90, 2023–2034 doi:10.3389/feart.2023.1217304

Kaya, M. Y., Dupont Nivet, G., Proust, J. N., Roperch, P., Bougeois, L., Meijer, N., et al. (2019). Paleogene evolution and demise of the proto Paratethys Sea in Central Asia (Tarim and Tajik basins): Role of intensified tectonic activity at ca 41 Ma. *Basin Res.* 31, 461–486. doi:10.1111/bre.12330

Kent-Corson, M. L., Ritts, B. D., Zhuang, G., Bovet, P. M., Graham, S. A., and Page Chamberlain, C. (2009). Stable isotopic constraints on the tectonic, topographic, and climatic evolution of the northern margin of the Tibetan Plateau. *Earth Planet. Sci. Lett.* 282, 158–166. doi:10.1016/j.epsl.2009.03.011

Kim, S., and O'Neil, J. R. (1997). Equilibrium and nonequilibrium oxygen isotope effects in synthetic carbonates. *Geochim. Cosmochim. Acta* 61, 3461–3475. doi:10.1016/S0016-7037(97)00169-5

Kutzbach, J. E., Guetter, P. J., Ruddiman, W. F., and Prell, W. L. (1989). Sensitivity of climate to late cenozoic uplift in southern Asia and the American west: Numerical experiments. *J. Geophys. Res. Atmos.* 94 (18), 18393–393. doi:10.1029/JD094iD15p18393

Lease, R. O., Burbank, D. W., Clark, M. K., Farley, K. A., Zheng Dewen, Z. D., and Zhang, H. (2011). Middle Miocene reorganization of deformation along the northeastern Tibetan Plateau. *Geol. (Boulder)* 39, 359–362. doi:10.1130/G31356.1

Leng, M. J., and Marshall, J. D. (2004). Palaeoclimate interpretation of stable isotope data from lake sediment archives. *Quat. Sci. Rev.* 23, 811–831. doi:10.1016/j.quascirev.2003.06.012

Li, B., Sun, D., Wang, X., Zhang, Y., Hu, W., Wang, F., et al. (2016a). δ18O and δ13C records from a Cenozoic sedimentary sequence in the Lanzhou Basin, Northwestern China: Implications for palaeoenvironmental and palaeoecological changes. *J. Asian Earth Sci.* 125, 22–36. doi:10.1016/j.jseaes.2016.05.010

Li, B., Yan, M., Zhang, W., Parés, J. M., Fang, X., Yang, Y., et al. (2020a). Magnetic fabric constraints on the cenozoic compressional strain changes in the northern Qaidam marginal thrust belt and their tectonic implications. *Tectonics* 39, 5989. doi:10.1029/2019TC005989

Li, B., Zuza, A. V., Chen, X., Hu, D., Shao, Z., Qi, B., et al. (2020b). Cenozoic multi-phase deformation in the Qilian Shan and out-of-sequence development of the northern Tibetan Plateau. *Tectonophysics* 782-783, 228423. doi:10.1016/j.tecto.2020.228423

Li, H. C., and Ku, T. L. (1997). δ13C–δ18C covariance as a paleohydrological indicator for closed-basin lakes. *Palaeogeogr. Palaeoclimatol. Palaeoecol.* 133, 69–80. doi:10.1016/S0031-0182(96)00153-8

Li, J., Yue, L. P., Roberts, A. P., Hirt, A. M., Pan, F., Guo, L., et al. (2018a). Global cooling and enhanced Eocene Asian mid-latitude interior aridity. *Nat. Commun.* 9, 3026. doi:10.1038/s41467-018-05415-x

Li, L., Fan, M., Davila, N., Jesmok, G., Mitsunaga, B., Tripati, A., et al. (2018c). Carbonate stable and clumped isotopic evidence for late Eocene moderate to high elevation of the east-central Tibetan Plateau and its geodynamic implications. *GSA Bull.* 131, 831–844. doi:10.1130/B32060.1

Li, L., Garzione, C. N., Pullen, A., and Chang, H. (2016b). Early–middle Miocene topographic growth of the northern Tibetan Plateau: Stable isotope and sedimentation evidence from the southwestern Qaidam basin. *Palaeogeogr. Palaeoclimatol. Palaeoecol.* 461, 201–213. doi:10.1016/j.palaeo.2016.08.025

Li, L., Wu, C., Fan, C., Li, J., and Zhang, C. (2017). Carbon and oxygen isotopic constraints on paleoclimate and paleoelevation of the southwestern Qaidam basin, northern Tibetan Plateau. *Geosci. Front.* 8, 1175–1186. doi:10.1016/j.gsf.2016.12.001

Li, M., Sun, S., Fang, X., Wang, C., Wang, Z., and Wang, H. (2018b). Clay minerals and isotopes of pleistocene lacustrine sediments from the Western Qaidam Basin, NE Tibetan plateau. *Appl. Clay Sci.* 162, 382–390. doi:10.1016/j.clay.2018.06.033

Liu, D., Li, H., Sun, Z., Pan, J., Wang, M., Wang, H., et al. (2017). AFT dating constrains the cenozoic uplift of the qimen tagh mountains, northeast Tibetan plateau, comparison with LA-ICPMS zircon U–Pb ages. *Gondwana Res.* 41, 438–450. doi:10.1016/j.gr.2015.10.008

Liu, Z., Zhang, Y., Song, G., Li, S., Long, G., Zhao, J., et al. (2021). Mixed carbonate rocks lithofacies features and reservoirs controlling mechanisms in a saline lacustrine basin in Yingxi area, Qaidam Basin, NW China. *PETROLEUM Explor. Dev.* 48, 80–94. doi:10.1016/S1876-3804(21)60006-X

Long, L., Fang, X., Miao, Y., Bai, Y., and Wang, Y. (2011). Northern Tibetan Plateau cooling and aridification linked to Cenozoic global cooling: Evidence from n-alkane distributions of Paleogene sedimentary sequences in the Xining Basin. *Chin. Sci. Bull.* 56, 1569–1578. doi:10.1007/s11434-011-4469-0

Lu, H., and Xiong, S. (2009). Magnetostratigraphy of the Dahonggou section, northern Qaidam Basin and its bearing on cenozoic tectonic evolution of the qilian Shan and Altyn tagh fault. *Earth Planet. Sci. Lett.* 288, 539–550. doi:10.1016/j.epsl.2009.10.016

Lv, F., Liu, C., Jiao, P., Zhang, H., Sun, X., and Zhang, Y. (2018). Carbon and oxygen isotopic compositions of the lacustrine carbonate in Lop Nur since the mid-pleistocene and their paleoenvironment significance. *Acta Geol. Sin.* 26, 87–91.

Ma, J., Wu, C., Wang, Y., Wang, J., Fang, Y., Zhu, W., et al. (2017). Paleoenvironmental reconstruction of a saline lake in the Tertiary: Evidence from aragonite laminae in the northern Tibet Plateau. *Sediment. Geol.* 353, 1–12. doi:10.1016/j.sedgeo.2017.03.002

Macaulay, E. A., Sobel, E. R., Mikolaichuk, A., Wack, M., Gilder, S. A., Mulch, A., et al. (2016). The sedimentary record of the issyk Kul basin, Kyrgyzstan: Climatic and tectonic inferences. *Basin Res.* 28, 57–80. doi:10.1111/bre.12098

Manabe, S., and Broccoli, A. J. (1990). Mountains and arid climates of middle latitudes. *Science* 247, 192–195. doi:10.1126/science.247.4939.192

Meijer, N., Dupont-Nivet, G., Abels, H. A., Kaya, M. Y., Licht, A., Xiao, M., et al. (2019). Central Asian moisture modulated by proto-Paratethys Sea incursions since the early Eocene. *Earth Planet. Sci. Lett.* 510, 73–84. doi:10.1016/j.epsl.2018.12.031

Miao, Y., Fang, X., Herrmann, M., Wu, F., Zhang, Y., and Liu, D. (2011). Miocene pollen record of KC-1 core in the Qaidam Basin, NE Tibetan Plateau and implications for evolution of the East Asian monsoon. *Palaeogeogr. Palaeoclimatol. Palaeoecol.* 299, 30–38. doi:10.1016/j.palaeo.2010.10.026

Miao, Y., Fang, X., Liu, Y. C., Yan, X., Li, S., and Xia, W. (2016). Late Cenozoic pollen concentration in the Western Qaidam Basin, northern Tibetan Plateau, and its significance for paleoclimate and tectonics. *Rev. Palaeobot. Palynol.* 231, 14–22. doi:10.1016/j.revpalbo.2016.04.008

Miao, Y., Fang, X., Wu, F., Cai, M., Song, C., Meng, Q., et al. (2013). Late cenozoic continuous aridification in the Western Qaidam Basin: Evidence from sporopollen records. *Clim. Past.* 9, 1863–1877. doi:10.5194/cp-9-1863-2013

Miller, K. G., Browning, J. V., Schmelz, W. J., Kopp, R. E., Mountain, G. S., and Wright, J. D. (2020). Cenozoic sea-level and cryospheric evolution from deep-sea geochemical and continental margin records. *Sci. Adv.* 6, 1346. doi:10.1126/sciadv.aaz1346

Nie, J., Ren, X., Saylor, J. E., Su, Q., Horton, B. K., Bush, M. A., et al. (2019). Magnetic polarity stratigraphy, provenance, and paleoclimate analysis of Cenozoic strata in the Qaidam Basin, NE Tibetan Plateau. *GSA Bull.* 132, 310–320. doi:10.1130/B35175.1

O'Neil, J. R., Clayton, R. N., and Mayeda, T. K. (1969). Oxygen isotope fractionation in divalent metal carbonates. *J. Chem. Phys.* 51, 5547–5558. doi:10.1063/1.1671982

Page, M., Licht, A., Dupont-Nivet, G., Meijer, N., Barbolini, N., Hoorn, C., et al. (2019). Synchronous cooling and decline in monsoonal rainfall in northeastern Tibet during the fall into the Oligocene icehouse. *Geology* 47, 203–206. doi:10.1130/G45480.1

Pan, Y. (1999). Formation and uplifting of the qinghai–tibet plateau. *Earth Sci. Front.* 1999, 153–163.

Ramstein, G., Fluteau, F., Besse, J., and Joussaume, S. (1997). Effect of orogeny, plate motion and land–sea distribution on Eurasian climate change over the past 30 million years. *Nature* 386, 788–795. doi:10.1038/386788a0

Ricketts, R. D., and Anderson, R. F. (1998). A direct comparison between the historical record of lake level and the $\delta^{18}O$ signal in carbonate sediments from Lake Turkana, Kenya. *Limnol. Oceanogr.* 43, 811–822. doi:10.4319/lo.1998.43.5.0811

Rieser, A. B., Bojar, A., Neubauer, F., Genser, J., Liu, Y., Ge, X., et al. (2009). Monitoring cenozoic climate evolution of northeastern Tibet: Stable isotope constraints from the Western Qaidam Basin, China. *Int. J. Earth Sci.* 98, 1063–1075. doi:10.1007/s00531-008-0304-5

Ritter, A., Mavromatis, V., Dietzel, M., Kwiecien, O., Wiethoff, F., Griesshaber, E., et al. (2017). Exploring the impact of diagenesis on (isotope) geochemical and microstructural alteration features in biogenic aragonite. *Sedimentology* 64, 1354–1380. doi:10.1111/sed.12356

Rowley, D. B., and Currie, B. S. (2006). Palaeo-altimetry of the late Eocene to Miocene Lunpola basin, central Tibet. *Nature* 439, 677–681. doi:10.1038/nature04506

Ruddiman, W. F., and Kutzbach, J. E. (1989). Forcing of late Cenozoic northern hemisphere climate by plateau uplift in southern Asia and the American west. *J. Geophys. Res.* 94, 18409. doi:10.1029/JD094iD15p18409

Saez, A., and Cabrera, L. (2002). Sedimentological and palaeohydrological responses to tectonics and climate in a small, closed, lacustrine system: Oligocene as Pontes Basin (Spain). *Sedimentology* 49, 1073–1094. doi:10.1046/j.1365-3091.2002.00490.x

Song, B., Ji, J., Wang, C., Xu, Y., and Zhang, K. (2017). Intensified aridity in the Qaidam Basin during the middle Miocene: Constraints from ostracod, stable isotope, and weathering records. *Can. J. Earth Sci.* 54, 242–256. doi:10.1139/cjes-2016-0052

Song, B., Spicer, R. A., Zhang, K., Ji, J., Farnsworth, A., Hughes, A. C., et al. (2020). Qaidam Basin leaf fossils show northeastern Tibet was high, wet and cool in the early Oligocene. *Earth Planet. Sci. Lett.* 537, 116175. doi:10.1016/j.epsl.2020.116175

Song, B., Zhang, K., Lu, J., Wang, C., and Xu, Y. (2013). The middle Eocene to early Miocene integrated sedimentary record in the Qaidam Basin and its implications for paleoclimate and early Tibetan Plateau uplift. *Can. J. Earth Sci.* 50, 183–196. doi:10.1139/cjes-2012-0048

Song, C., Hu, S., Han, W., Zhang, T., Fang, X., Gao, J., et al. (2014). Middle Miocene to earliest Pliocene sedimentological and geochemical records of climate change in the

Western Qaidam Basin on the NE Tibetan Plateau. *Palaeogeogr. Palaeoclimatol. Palaeoecol.* 395, 67–76. doi:10.1016/j.palaeo.2013.12.022

Sun, Y., Liu, J., Liang, Y., Ji, J., Liu, W., Aitchison, J. C., et al. (2020). Cenozoic moisture fluctuations on the northeastern Tibetan Plateau and association with global climatic conditions. *J. Asian Earth Sci.* 200, 104490. doi:10.1016/j.jseaes.2020.104490

Sun, Z. M., Yang, Z. Y., Pei, J. L., Ge, X. H., Wang, X. S., Yang, T. S., et al. (2005). Magnetostratigraphy of Paleogene sediments from northern Qaidam Basin, China: Implications for tectonic uplift and block rotation in northern Tibetan plateau. *Earth Planet. Sci. Lett.* 237, 635–646. doi:10.1016/j.epsl.2005.07.007

Talbot, M. R. (1990). A review of the palaeohydrological interpretation of carbon and oxygen isotopic ratios in primary lacustrine carbonates. *Chem. Geol. Isot. Geosci. Sect.* 80, 261–279. doi:10.1016/0168-9622(90)90009-2

Tapponnier, P., Zhiqin, X., Roger, F., Meyer, B., Arnaud, N., Wittlinger, G., et al. (2001). Oblique stepwise rise and growth of the Tibet plateau. *Science* 294, 1671–1677. doi:10.1126/science.105978

Wang, C. L., Liu, C. L., Ming, X. H., Wang, L. C., and Zhang, L. B. (2013). S genotyping in Japanese plum and sweet cherry by allele-specific hybridization using streptavidin-coated magnetic beads. *Acta Geosci. Sin.* 34, 567–576. doi:10.1007/s00299-013-1388-3

Wang, C., Zhao, X., Liu, Z., Lippert, P. C., Graham, S. A., Coe, R. S., et al. (2008). Constraints on the early uplift history of the Tibetan Plateau. *Proc. Natl. Acad. Sci.* 105, 4987–4992. doi:10.1073/pnas.0703595105

Wang, F., Feng, H., Shi, W., Zhang, W., Wu, L., Yang, L., et al. (2016). Relief history and denudation evolution of the northern Tibet margin: Constraints from 40Ar/39Ar and (U–Th)/He dating and implications for far-field effect of rising plateau. *Tectonophysics* 675, 196–208. doi:10.1016/j.tecto.2016.03.001

Wang, J., Wang, Y. J., Liu, Z. C., Li, J. Q., and Xi, P. (1999). Cenozoic environmental evolution of the Qaidam Basin and its implications for the uplift of the Tibetan Plateau and the drying of central Asia. *Palaeogeogr. Palaeoclimatol. Palaeoecol.* 152, 37–47. doi:10.1016/S0031-0182(99)00038-3

Wang, W., Zheng, W., Zhang, P., Li, Q., Kirby, E., Yuan, D., et al. (2017). Expansion of the Tibetan plateau during the neogene. *Nat. Commun.* 8, 15887. doi:10.1038/ncomms15887

Wang, X., Carrapa, B., Chapman, J. B., Henriquez, S., Wang, M., DeCelles, P. G., et al. (2019). Parathethys last gasp in central Asia and late Oligocene accelerated uplift of the pamirs. *Geophys. Res. Lett.* 46, 11773–11781. doi:10.1029/2019GL084838

Wang, X., Carrapa, B., Sun, Y., Dettman, D. L., Chapman, J. B., Caves Rugenstein, J. K., et al. (2020). The role of the westerlies and orography in Asian hydroclimate since the late Oligocene. *Geology* 48, 728–732. doi:10.1130/G47400.1

Wang, Y., Zheng, J., Zhang, W., Li, S., Liu, X., Yang, X., et al. (2012). Cenozoic uplift of the Tibetan plateau: Evidence from the tectonic–sedimentary evolution of the Western Qaidam Basin. *Geosci. Front.* 3, 175–187. doi:10.1016/j.gsf.2011.11.005

Westerhold, T., Marwan, N., Drury, A. J., Liebrand, D., Agnini, C., Anagnostou, E., et al. (2020). An astronomically dated record of Earth's climate and its predictability over the last 66 million years. *Science* 369, 1383–1387. doi:10.1126/science.aba6853

Wu, C., Li, J., and Ding, L. (2021). Low-temperature thermochronology constraints on the evolution of the eastern Kunlun range, northern Tibetan plateau. *Geosphere* 17, 1193–1213. doi:10.1130/GES02358.1

Wu, F., Fang, X., Yang, Y., Dupont-Nivet, G., Nie, J., Fluteau, F., et al. (2022). Reorganization of Asian climate in relation to Tibetan Plateau uplift. *Nat. Rev. Earth Environ.* 3, 684–700. doi:10.1038/s43017-022-00331-7

Wu, M., Zhuang, G., Hou, M., and Miao, Y. (2019). Ecologic shift and aridification in the northern Tibetan Plateau revealed by leaf wax n-alkane δ2H and δ13C records. *Palaeogeogr. Palaeoclimatol. Palaeoecol.* 514, 464–473. doi:10.1016/j.palaeo.2018.11.005

Xiao, G. Q., Abels, H. A., Yao, Z. Q., Dupont-Nivet, G., and Hilgen, F. J. (2010). Asian aridification linked to the first step of the Eocene-Oligocene climate Transition (EOT) in obliquity-dominated terrestrial records (Xining Basin, China). *Clim. Past.* 6, 501–513. doi:10.5194/cp-6-501-2010

Xiong, Y., Tan, X., Wu, K., Xu, Q., Liu, Y., and Qiao, Y. (2021). Petrogenesis of the Eocene lacustrine evaporites in the Western Qaidam Basin: Implications for regional tectonic and climate changes. *Sediment. Geol.* 416, 105867. doi:10.1016/j.sedgeo.2021.105867

Xiong, Z., Ding, L., Spicer, R. A., Farnsworth, A., Wang, X., Valdes, P. J., et al. (2020). The early Eocene rise of the Gonjo Basin, SE Tibet: From low desert to high forest. *Earth Planet. Sci. Lett.* 543, 116312. doi:10.1016/j.epsl.2020.116312

Xiong, Z., Liu, X., Ding, L., Farnsworth, A., Spicer, R. A., Xu, Q., et al. (2022). The rise and demise of the paleogene central Tibetan valley. *Sci. Adv.* 8, 0944. doi:10.1126/sciadv.abj0944

Ye, C., Yang, Y., Fang, X., and Zhang, W. (2016). Late Eocene clay boron-derived paleosalinity in the Qaidam Basin and its implications for regional tectonics and climate. *Sediment. Geol.* 346, 49–59. doi:10.1016/j.sedgeo.2016.10.006

Ye, C., Yang, Y., Fang, X., Zhang, W., Song, C., and Yang, R. (2020). Paleolake salinity evolution in the Qaidam Basin (NE Tibetan plateau) between ~42 and 29 Ma: Links to global cooling and Paratethys Sea incursions. *Sediment. Geol.* 409, 105778. doi:10.1016/j.sedgeo.2020.105778

Yi, H., Lin, J., Zhou, K., and Junfeng, L. (2007). Carbon and oxygen isotope characteristics and palaeoenvironmental implication of the Cenozoic lacustrine carbonate rocks in northern Qinghai-Tibetan Plateau. *J. Palaeogeogr.* 8, 1175–1186. doi:10.1016/S1872-5791(07)60044-X

Yin, A., and Harrison, T. M. (2000). Geologic evolution of the Himalayan-Tibetan orogen. *Annu. Rev. Earth Planet. Sci.* 28, 211–280. doi:10.1146/annurev.earth.28.1.211

Yuan, J., Huang, C., Zhao, F., and Pan, X. (2015). Carbon and oxygen isotopic compositions, and palaeoenvironmental significance of saline lacustrine dolomite from the Qaidam Basin, Western China. *J. Pet. Sci. Eng.* 135, 596–607. doi:10.1016/j.petrol.2015.10.024

Zachos, J. C., Dickens, G. R., and Zeebe, R. E. (2008). An early Cenozoic perspective on greenhouse warming and carbon-cycle dynamics. *Nature* 451, 279–283. doi:10.1038/nature06588

Zachos, J. C., and Kump, L. R. (2005). Carbon cycle feedbacks and the initiation of Antarctic glaciation in the earliest Oligocene. *Glob. Planet. Change* 47, 51–66. doi:10.1016/j.gloplacha.2005.01.001

Zachos, J., Pagani, M., Sloan, L., Thomas, E., and Billups, K. (2001). Trends, rhythms, and aberrations in global climate 65 Ma to present. *Science* 292, 686–693. doi:10.1126/science.1059412

Zhang, W., Jian, X., Fu, L., Feng, F., and Guan, P. (2018). Reservoir characterization and hydrocarbon accumulation in late Cenozoic lacustrine mixed carbonate-siliciclastic fine-grained deposits of the northwestern Qaidam basin, NW China. *Mar. Pet. Geol.* 98, 675–686. doi:10.1016/j.marpetgeo.2018.09.008

Zhang, W., Li, Z., Feng, F., Zhai, Z., Sun, W., Tang, C., et al. (2013). Carbon and oxygen isotopic composition of lacustrine carbonate rocks of the Lower-Middle Jurassic in NE part of central Sichuan Province and their palaeoenvironmental significance. *J. Palaeogeogr.* 15, 247–260.

Zhang, W. (2006). *The high precise Cenozoic magnetostratigraphy of the Qaidam Basin and uplift of the Northern Tibetan plateau*. Lanzhou: Lanzhou University.

Zhuang, G., Hourigan, J. K., Koch, P. L., Ritts, B. D., and Kent-Corson, M. L. (2011). Isotopic constraints on intensified aridity in Central Asia around 12Ma. *Earth Planet. Sci. Lett.* 312, 152–163. doi:10.1016/j.epsl.2011.10.005